The Motion of Hurricane Gloria: A Potential Vorticity Diagnosis

LLOYD J. SHAPIRO

Hurricane Research Division, AOML/NOAA, Miami, Florida

(Manuscript received 27 February 1996, in final form 21 May 1996)

ABSTRACT

Multilevel, multinested analyses of Hurricane Gloria of 1985 are the most comprehensive kinematic dataset yet developed for a single hurricane. A piecewise inversion technique is used with these analyses and the nonlinear balance equation to deduce the three-dimensional distribution of potential vorticity (PV) that contributed to the deep-layer mean (DLM) flow that steered Gloria toward the northwest. The background state is taken to be the azimuthally averaged winds in balance with a geopotential distribution on an f plane. Advantage is taken of the near-linearity of the weak asymmetries near the hurricane's core and of PV in the environment. Thus, ad hoc aspects of the linearization required by other investigators are effectively eliminated. Removal of the hurricane vortex and the use of a climatological mean background state are avoided as well. The insensitivity of the results to the imposed lateral boundary conditions is also demonstrated.

Wind anomalies attributable to pieces of anomalous PV restricted to cylinders of different radii centered on the hurricane are evaluated. The DLM wind that steered Gloria to the northwest is primarily attributable to PV anomalies confined within a cylinder of radius 1000 km and levels 500 mb and above, including positive anomalies associated with a cold low over Cuba. The vector difference between the hurricane's observed motion and the DLM wind at Gloria's center attributable to these PV anomalies is 1.0 m s^{-1}, explaining more than five-sixths of the hurricane's 6.2 m s^{-1} motion. Implications for measurements required to establish short-term changes of the environmental steering flow are considered. Difficulties in the interpretation of results are discussed for PV anomalies that are confined to noncircular regions; the implication for other studies is considered as well.

1. Introduction

a. Background

Hurricane motion is governed by an apparently complex interaction between the large-scale circulation in which the storm is embedded and the storm circulation itself, involving scales from the synoptic down to the convective. Larger spatial scales tend to influence longer-term motion. It is well established that the vertically averaged flow near a hurricane is an excellent indicator of subsequent 24-h motion (Franklin et al. 1996; also see review in section 2a of Wu and Emanuel 1995a). The factors that contribute to hurricane motion in a two-dimensional barotropic context, including the beta effect and horizontal vorticity gradients associated with the large-scale flow, are reasonably well understood (e.g., Shapiro and Ooyama 1990). The three-dimensional dynamics that determines hurricane motion is much less well established.

Studies with simple baroclinic models have deduced the importance of horizontal potential vorticity (PV) gradients (Shapiro 1992) or convectively induced upper-tropospheric PV anomalies (Wu and Emanuel 1993) in hurricane vortex propagation. Potential vorticity is the natural context in which to understand the three-dimensional dynamics. In the absence of diabatic and frictional effects, PV is conserved. Moreover, as articulated by Hoskins et al. (1985), once a balance condition, boundary conditions, and appropriate background state have been specified, PV can be inverted to derive the entire three-dimensional wind and temperature (pressure or geopotential height) distribution. These properties allow one, in principle, to isolate the physical factors that determine the three-dimensional wind field and thus hurricane motion.

Because of the general nonlinear nature of the PV and balance equation, analysis and interpretation can be difficult in practice. Thus, few studies have been made using the standard (Charney) balance equation. Davis and Emanuel (1991) applied an ad hoc linearization of the PV and balance equation. The linearization allowed them to decompose the PV field in a piecewise manner, using the PV inversion to deduce the relative contribution of various atmospheric layers to the evolution of a midlatitude cyclogenesis event. The utility of the piecewise inversion technique was evaluated more completely in Davis (1992). Wu and Emanuel (1995a,b) have recently used the technique to understand hurricane motion, finding that upper-level PV

Corresponding author address: Dr. Lloyd J. Shapiro, Hurricane Research Division, AOML/NOAA, 4301 Rickenbacker Causeway, Miami, FL 33149.

anomalies can have an important role in determining hurricane motion. As with Davis and Emanuel (1991), a climatological (time-mean) PV distribution was used to derive the wind and temperature of the background state. The inversion technique was then used to derive the wind and temperature anomalies that were associated with (or "attributed to") a given piece of anomalous PV. Since the background flow was specified, it remained inaccessible to decomposition. Moreover, due to the sensitivity of the results to the choice of the hurricane's center in Wu and Emanuel's analysis, the PV anomaly associated with the hurricane vortex itself had to be excluded.

In the present paper a piecewise inversion technique is used to deduce the three-dimensional distribution of PV that contributed to the deep-layer mean (DLM) flow that steered Hurricane Gloria of 1985. Specific questions to be addressed include: What atmospheric levels steered the storm? What spatial scales? Advantage will be taken of the near-linearity of the weak asymmetric disturbances in Gloria near the core and of PV in the environment (Shapiro and Montgomery 1993). Thus, ad hoc aspects of the linearization required by Davis and Emanuel (1991) and Wu and Emanuel (1995a,b) will be effectively eliminated. The removal of the hurricane vortex and the use of a climatological mean background state will be avoided as well.

Additional issues related to the interpretation of piecewise inversion have been raised by Bishop and Thorpe (1994) and Thorpe and Bishop (1995). As they note, unique attribution of a wind and temperature field to a given PV distribution requires not only that the anomalies be superposable (linear), but also that the results are insensitive to the choice of boundary conditions. Lateral boundaries in the present study will be shown to be sufficiently remote that this condition is satisfied. As discussed in section 3, issues regarding the upper and lower boundary conditions are more problematic.

b. Hurricane Gloria

Multilevel, multinested analyses of Hurricane Gloria, including Doppler winds near the storm's center and Omega dropwindsondes in its environment (Franklin et al. 1993), are the most comprehensive kinematic dataset yet developed for a single hurricane. The analysis domain covers essentially the entire western hemisphere from south of the equator to near the North Pole. The completed analyses utilize the spectral application of the finite element representation, developed by Ooyama (1987), on meshes with effective resolutions ranging from about 150 km down to 2.5 km in the hurricane's core. All 10 mandatory levels from 1000 to 100 mb, excluding 925 mb, are analyzed. The top panel of Fig. 1 displays the 100–1000-mb DLM winds, **u**, in the vicinity of the hurricane at the analysis time of 0000

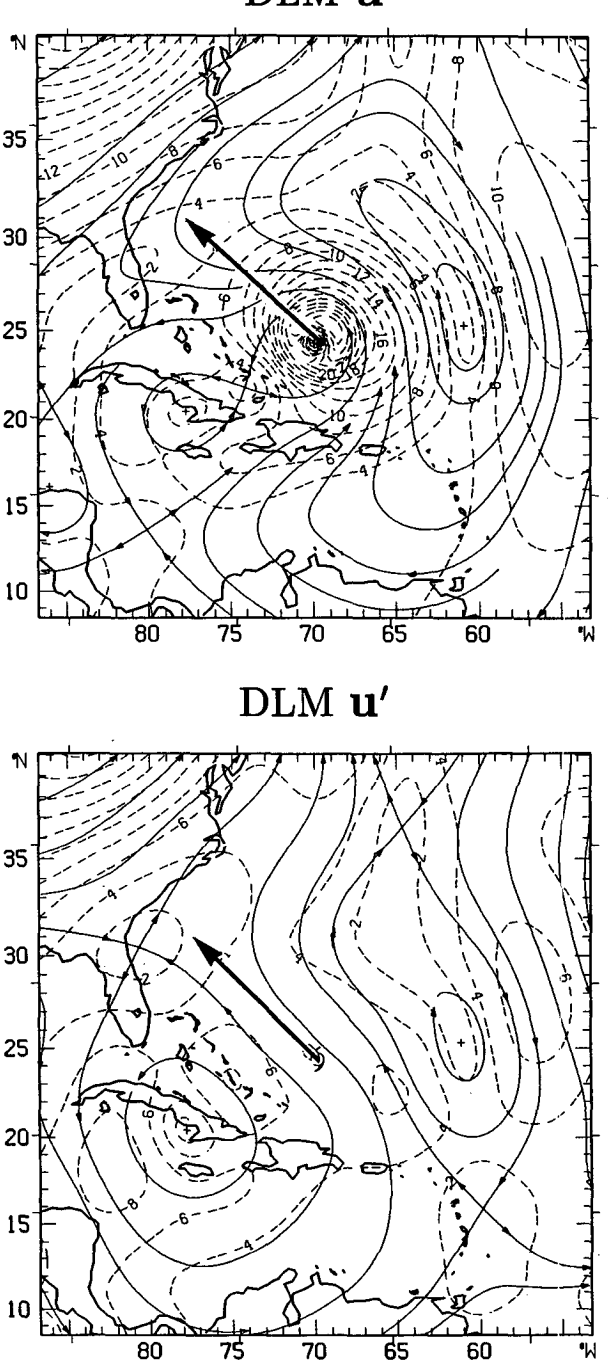

FIG. 1. Deep-layer mean (100–1000 mb) nondivergent winds (streamlines and isotachs; contour interval 2 m s^{-1}). Hurricane symbol is at Gloria's center. Total winds **u** (top panel) and asymmetric winds **u′** (bottom panel) are shown. Analyses use a horizontal low-pass filter with a minimum 45-km spatial scale. Vector in top panel indicates hurricane's mean motion and in bottom panel the deep-layer mean wind at the center of the vortex.

UTC 25 September 1985. Only the nondivergent part of the wind is used, derived from the vorticity and the constraint that there is no net divergence out of the full domain (depicted in top panel of Fig. 2). The analysis shown in Fig. 1 uses a horizontal low-pass filter with a minimum 45-km spatial scale. On this scale the wind is, in fact, nearly nondivergent. The storm circulation is embedded in a flow that includes cyclonic and anticyclonic gyres to the southwest and northeast of the hurricane, respectively. During the 12 h centered on the analysis time, the hurricane's mean motion was toward the northwest at 6.2 m s^{-1}. The bottom panel of Fig. 1 displays the asymmetric wind, $\mathbf{u}' \equiv \mathbf{u} - \bar{\mathbf{u}}$, where $\bar{\mathbf{u}}$ is the wind averaged azimuthally about the vortex center. Since the wind is nondivergent, $\bar{\mathbf{u}}$ is strictly tangential. The opposing gyres and the flow across the vortex that advected it to the northwest are more clearly seen. Consistent with the analysis of Shapiro and Montgomery (1993), the asymmetries are quite weak within the hurricane's circulation. In the present (45-km scale) analysis, the DLM wind at the center of the hurricane vortex had a magnitude of 6.1 m s^{-1} and a vector difference from the storm's motion of only 0.2 m s^{-1}.

Recently, Shapiro and Franklin (1995, hereafter SF) used the wind analyses of Hurricane Gloria to derive the PV distribution. Since three-dimensional geopotential (or temperature) fields required for the evaluation of PV were not available in the hurricane core, they were derived using the standard balance equation. The resulting depiction of PV was the first presented for a real hurricane. The large-scale distribution of Ertel's PV, presented on isentropic surfaces (Fig. 8 of SF), evidenced asymmetries (Fig. 9 of SF) that appeared to be associated with Gloria's northwestward translation. The top panel of Fig. 2 displays Ertel's PV at 200 mb, derived using geopotential heights determined from the standard nonlinear balance equation [Eq. (3-81) of Haltiner and Williams 1980; cf. Eq. (A2) of appendix] with heights specified on the designated domain boundaries. Ertel's PV is defined as

$$q = \frac{1}{\rho}\boldsymbol{\eta}\cdot\nabla\theta,$$

where ρ is the density, $\boldsymbol{\eta}$ the three-dimensional absolute vorticity vector, θ the potential temperature,[1] and ∇ the three-dimensional gradient operator. Large PV maxima associated with midlatitude troughs are seen over North America and the Atlantic. The region near the hurricane (bottom panel of Fig. 2) has a local PV maximum to the southwest of the center that is associated with an upper-level cold low over Cuba and low PV in all other quadrants. It was suggested by SF that the low PV might be convectively induced in the hurricane's outflow, as described by Wu and Emanuel (1993). The PV maximum associated with the cold low is much weaker at 500 mb (top panel of Fig. 3) and has disappeared by 850 mb (bottom panel of Fig. 3). The PV minimum to the east of the vortex is present at both these levels, demonstrating that it is not solely due to the hurricane's outflow and also that it may be partly associated with interactions between the vortex and the northward gradient of planetary vorticity [beta gyres; see, e.g., Shapiro 1992; Franklin et al. (1996)].

c. *Outline*

The PV features in Figs. 2 and 3, which were also seen in SF's isentropic analyses, appear to contribute to the gyre structure in Fig. 1 and thus to Gloria's motion. As noted by SF, however, a piecewise inversion is required to infer the contribution of PV at each level to the steering flow. Section 2 presents the decomposition of the wind, geopotential, and PV into background state and anomaly that is required for the piecewise inversion. The contribution of nonlinearities to the PV is evaluated a priori. The piecewise inversion technique itself is developed in section 3, and results using PV anomalies restricted to cylindrical domains are presented. The contribution of the nonlinearities is shown in fact to be very small. The insensitivity of the results to the imposed lateral boundary conditions is also demonstrated. The section concludes with an evaluation of the contribution of the PV anomalies at each level to the total steering flow. Section 4 discusses the results, including problems of interpretation for PV anomalies not restricted to cylindrical domains.

2. Decomposition

As shown in Fig. 1, the asymmetric wind $\mathbf{u}'$ is much weaker than the total wind $\mathbf{u}$ in the near-vortex region. This observation, together with the tendency of the flow outside this region to be quasigeostrophic, allowed Shapiro and Montgomery (1993) to develop a balance formulation that links the highly rotational regime near the hurricane with the outer environment in a uniform manner. If the basic state is taken to be the azimuthally averaged (and therefore symmetric) vortex, then the anomalies are either weak asymmetries on the vortex or are in the quasigeostrophic regime. In either case the PV is linear. In the present formulation this same decomposition ($\mathbf{u} = \bar{\mathbf{u}} + \mathbf{u}'$) will be employed.

Under the assumption that the horizontal wind is nondivergent, the balance equation can be used to derive the geopotential height distribution ϕ from the streamfunction ψ. The nonlinear balance equation [Eq. (A2)] can be written schematically as

$$\nabla^2\phi = \nabla\cdot(f\nabla\psi) + B(\psi, \psi), \qquad (1)$$

where f is the Coriolis parameter and B is a nonlinear operator. The streamfunction anomaly ψ' is defined just as for the wind:

[1] Strictly speaking, θ is the virtual potential temperature, including the effect of moisture on density.

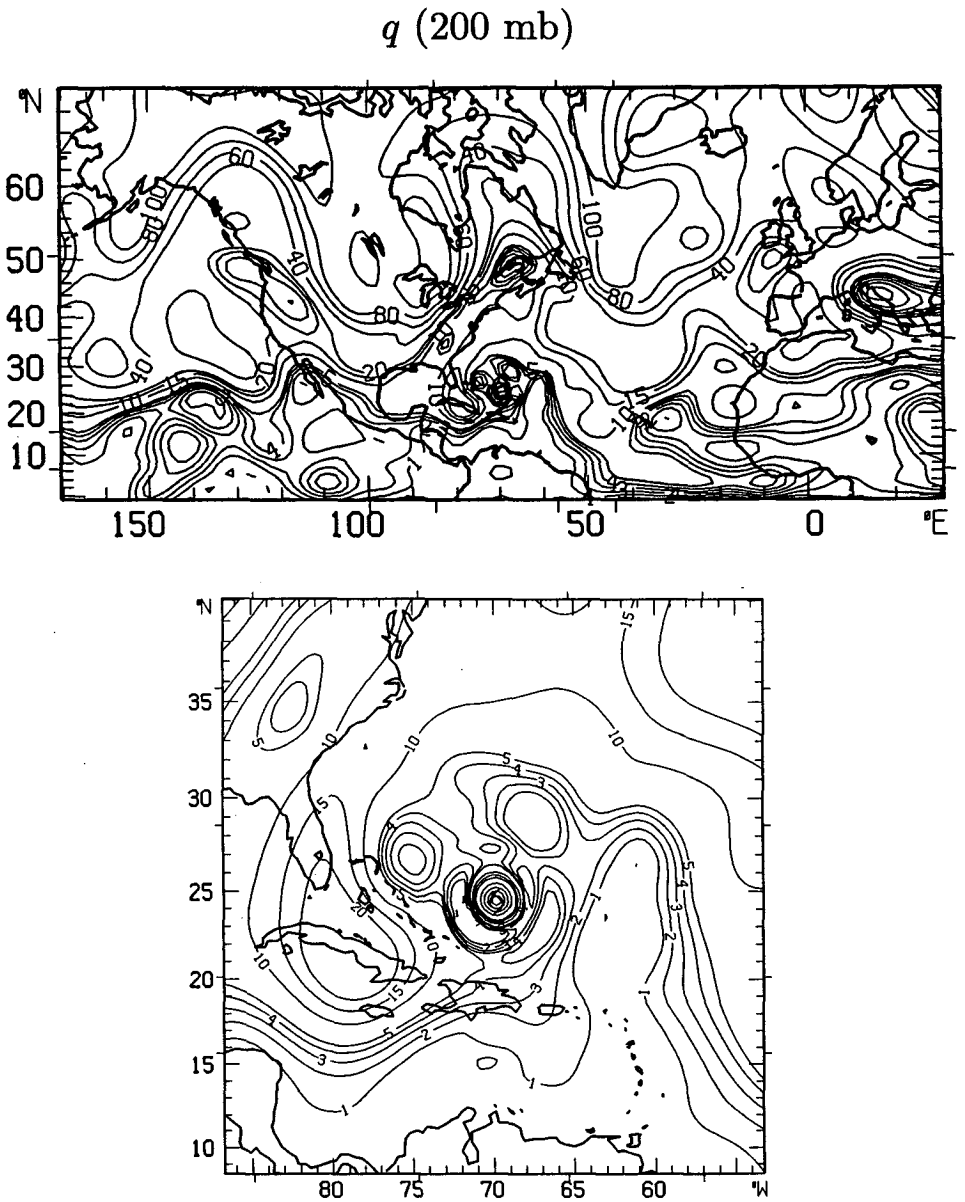

FIG. 2. Potential vorticity q at 200 mb. Contours are -1, 0, 1, 2, 3, 4, 5, 10, 15, 20, 40, 60, 80, 100 $\times 10^{-7}$ m^2 s^{-1} K kg^{-1}.

$$\psi' = \psi - \bar{\psi},$$

where $\bar{\psi}$ is the azimuthally averaged streamfunction.[2] The basic-state geopotential, $\hat{\phi}$, is taken to be in balance on an f plane with the azimuthally averaged winds, thereby satisfying

$$\nabla^2\hat{\phi} = \nabla\cdot(f_0\nabla\bar{\psi}) + B(\bar{\psi}, \bar{\psi}), \qquad (2)$$

where f_0 is the Coriolis parameter at the vortex center. In general, $\hat{\phi}$ is *not* the azimuthally averaged geopotential. In a symmetric domain with symmetric boundary conditions, $\hat{\phi}$ would be in symmetric gradient balance with the azimuthally averaged tangential wind. In practice the boundary values of $\hat{\phi}$, which are taken to be $\bar{\phi}$, the azimuthal average of ϕ, are on the rectangular domain (top panel of Fig. 2).[3] The geopotential anomaly, ϕ', is defined as the deviation from the basic state:

[2] Part of the circle on which the azimuthal average is derived may fall outside of the full domain (top panel of Fig. 2). In that case the average is restricted to points lying within the domain.

[3] Footnote 2 applies here as well.

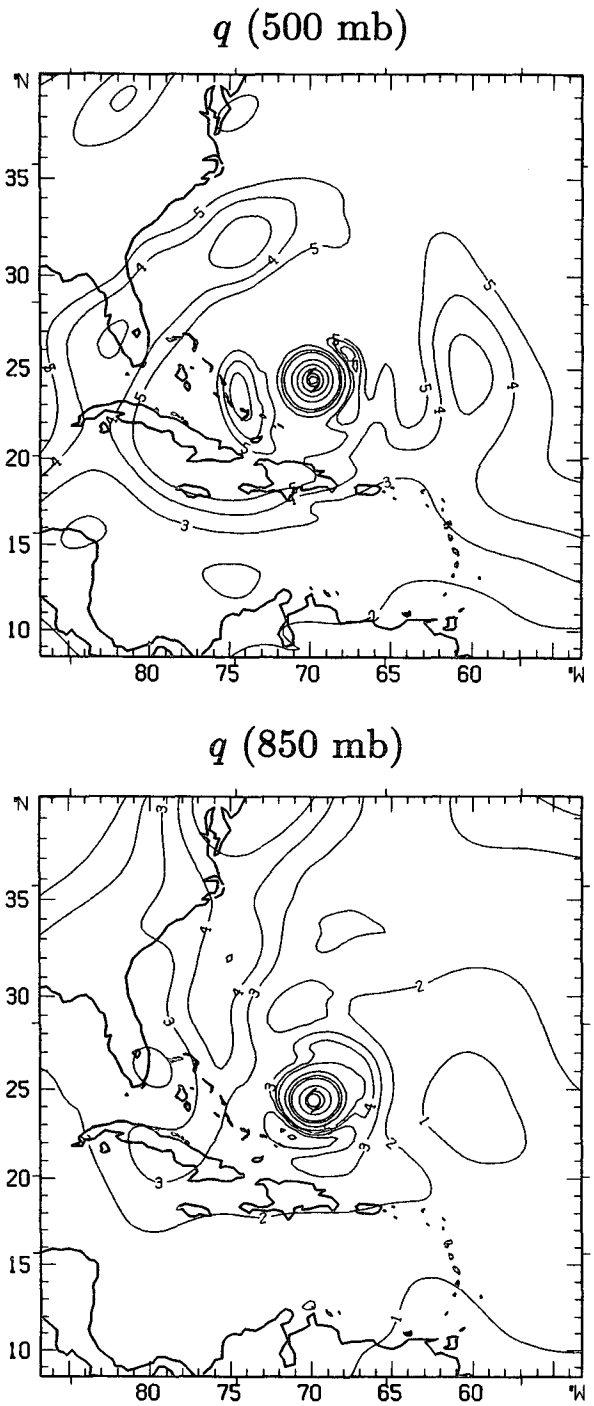

FIG. 3. Same as Fig. 2 but for potential vorticity at 500 mb (top panel) and 850 mb (bottom panel).

$$\phi' = \phi - \hat{\phi}.$$

For a nondivergent flow, Ertel's potential vorticity can be written as the sum of a linear function of ϕ and a nonlinear function of ψ and ϕ [Eq. (A1)]:

$$q = L(\phi) + Q(\psi, \phi).$$

The PV of the basic state is

$$\hat{q} = L(\hat{\phi}) + Q(\bar{\psi}, \hat{\phi}),$$

and the anomalies are defined by

$$q' = q - \hat{q}.$$

The top panel of Fig. 4 shows the basic-state PV at 200 mb. Although quite symmetric near the hurricane, $\hat{q}$ evidences asymmetries associated with both the northward gradient of the Coriolis parameter and the asymmetry in $\hat{\phi}$. The 200-mb PV anomaly, shown in the bottom panel of Fig. 4, has positive values in the region of the cold low over Cuba and mostly negative values elsewhere.

The PV anomaly, which may be rewritten

$$q' = L(\phi') + Q(\bar{\psi}, \phi') + Q(\psi', \hat{\phi}) + Q(\psi', \phi'), \quad (3)$$

comprises four parts. The first three terms in (3) are linear in the anomalies, while the fourth is nonlinear. Figure 5 shows q' at 200 mb, *excluding* the nonlinear term. Comparison with the bottom panel of Fig. 4 indicates that the nonlinearities contribute only a small amount to the PV anomaly. The contribution of nonlinearities to the results of a piecewise inversion will be evaluated in section 3b.

3. Piecewise inversion

a. Formulation and technique

Piecewise inversion decomposes the PV anomalies into "pieces" and associates each piece with a part of the wind and temperature anomaly fields. The association is made by inverting the coupled PV and balance equations for the streamfunction and geopotential anomalies, using appropriate boundary conditions. The PV equation for the anomalies was given schematically in (3), while the corresponding balance equation can [from (1) and (2)] be written

$$\nabla^2\phi' = \nabla\cdot[(f - f_0)\nabla\bar{\psi}] + \nabla\cdot(f\nabla\psi') + B(\bar{\psi}, \psi') + B(\psi', \bar{\psi}) + B(\psi', \psi'). \quad (4)$$

If the PV and balance equations (3) and (4) were linear, then the association of a piece of anomalous PV—q_i', with streamfunction and geopotential anomalies, ψ_i' and ϕ_i'—would be unique (at least in principle). Because of the general nonlinear nature of the system, Davis and Emanuel (1991) formulated an ad hoc partitioning that effectively linearizes the equations. Wu and Emanuel (1995a,b) used the same procedure in their analysis. Using Davis and Emanuel's (1991) partitioning, which is symmetric in its treatment of ψ and ϕ, the equations for the pieces of PV, ψ', and ϕ' can be written

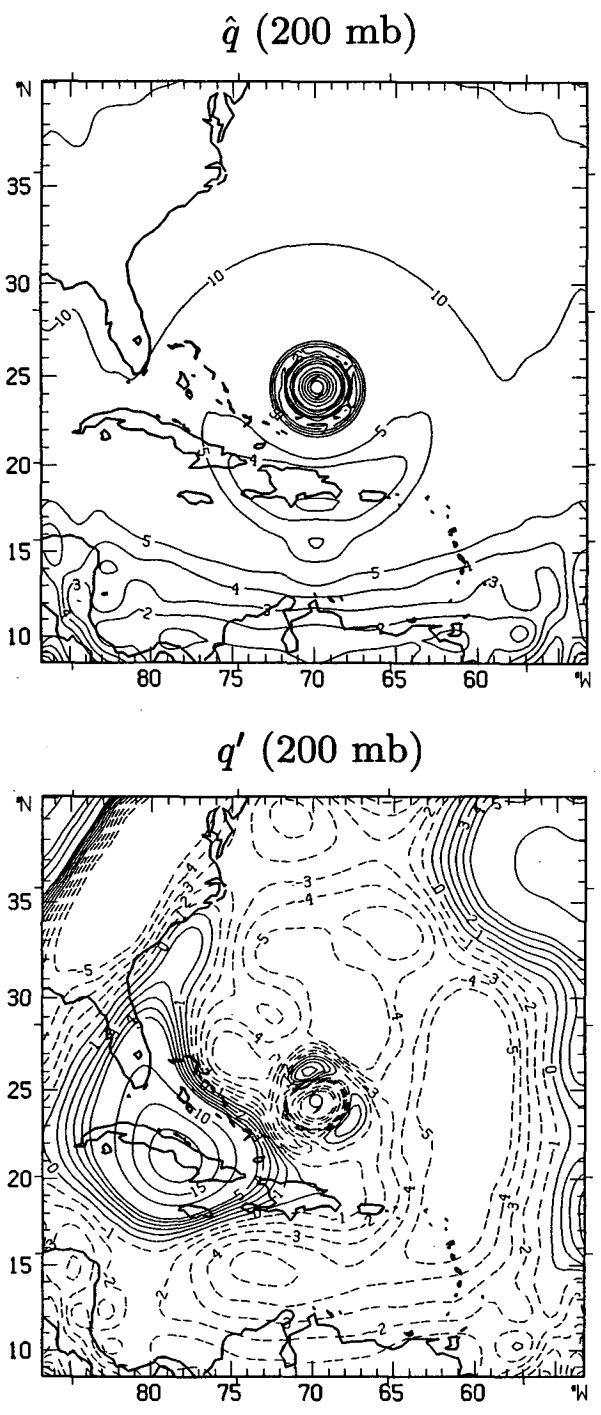

FIG. 4. Same as Fig. 2 but for basic-state potential vorticity $\hat{q}$ (top panel) and potential vorticity anomaly q' (bottom panel) at 200 mb.

$$q_i' = L(\phi_i') + Q\left(\bar{\psi} + \frac{1}{2}\psi', \phi_i'\right) + Q\left(\psi_i', \hat{\phi} + \frac{1}{2}\phi'\right), \quad (5a)$$

and [neglecting the very small contribution from the first term in (4)]

$$\nabla^2\phi_i' = \nabla\cdot(f\nabla\psi_i') + B\left(\bar{\psi} + \frac{1}{2}\psi', \psi_i'\right) + B\left(\psi_i', \bar{\psi} + \frac{1}{2}\psi'\right). \quad (5b)$$

The partitioning used in (5) is additive in the sense that the sum of all the pieces equals the whole. As will be demonstrated below, the nonlinear terms in (5) have a very small effect on the results of the present analysis.

The solution of the coupled system (5) requires the specification of boundary conditions. As noted by Davis and Emanuel (1991), homogeneous conditions are required on the lateral boundaries since the contribution of each piece of PV to the boundary winds and geopotentials is not known. The lateral boundaries will be shown to have a very small effect on the results of the present analysis. As was noted in section 1a, the interpretation of top and bottom boundary conditions is more problematic. In the present analysis potential temperature θ and, correspondingly (in a thermal wind sense), vertical shear are specified on the upper and lower boundaries. As noted by Bishop and Thorpe (1994), these conditions are commonly used [as in Davis and Emanuel (1991) and Wu and Emanuel (1995a,b)], probably due to the conservative nature of θ (cf. Hoskins 1991) as well as the demonstrated equiv-

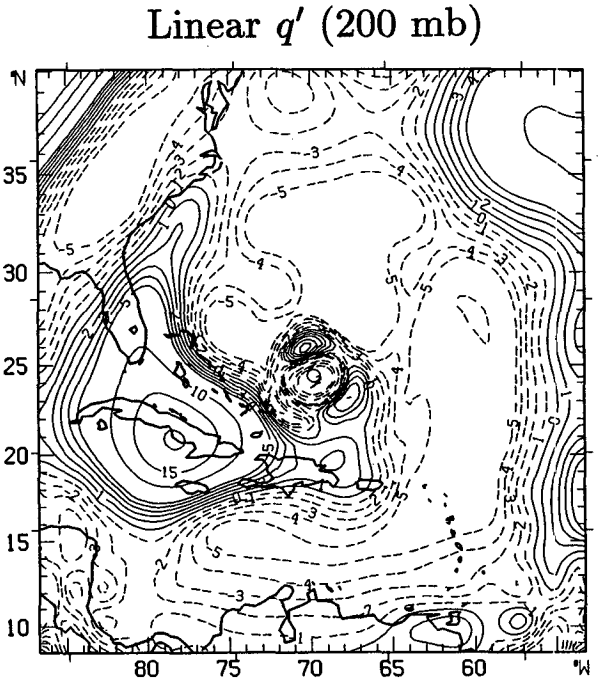

FIG. 5. Same as Fig. 2 but for potential vorticity anomaly q' at 200 mb, including only linear terms (see text).

alence of boundary θ to PV anomalies in baroclinic instability (Bretherton 1966a,b). Sensitivity of the results of the present paper to different upper or lower boundary conditions will not be explored.

The algorithm used to solve the coupled system (5) is similar to that used by Davis and Emanuel (1991, their appendix A). Salient details of the method are presented in the appendix.

b. Results

Figure 6 shows a piece of anomalous PV, q_i', at 200 mb, confined within a disk of radius 1000 km centered on the hurricane. This disk includes the substantial part of the upper cold low over Cuba (cf. Fig. 2). As a benchmark example, the DLM wind asymmetries, $\mathbf{u}_i'$, attributable to PV anomalies confined within a cylinder of this radius, and extending throughout the depth of the atmosphere, are shown in Fig. 7. Homogeneous lateral boundary conditions, $\psi_i' = 0$ and $\phi_i' = 0$, are applied on the indicated boundaries in the top panel of Fig. 7. Consistent with the discussion in section 3a, the vertical derivatives $\partial\psi_i'/\partial\pi$ and $\partial\phi_i'/\partial\pi$ $(=\theta_i')$, where π is the Exner function (see appendix), are specified on the upper (100 mb) and lower (1000 mb) boundaries. These quantities are taken to be the observed values within the 1000-km-radius cylinder and zero outside. Due to the elliptic character of the inversion, the DLM wind anomalies in the top panel of Fig. 7 extend throughout the domain. The DLM wind outside of the 1000-km-radius cylinder is weak, however. The wind near the vortex, shown in the bottom panel of Fig. 7, comprises a pair of counterrotating gyres with a northwestward component across Gloria's center. The DLM wind attributable to the PV anomalies is, in fact, very similar to the observed asymmetric DLM wind (bottom panel of Fig. 1). The vector difference between the DLM wind at the center of the vortex attributable to the PV anomalies and the observed motion of Gloria is 1.1 m s^{-1}.

The sensitivity of the results to the choice of lateral boundary conditions has been evaluated. The top panel of Fig. 8 shows the DLM wind near the vortex associated with the same piece of anomalous PV used to derive Fig. 7, but with boundary conditions on the northern and southern boundaries replaced by $\partial\psi_i'/\partial y = 0$ and $\partial\phi_i'/\partial y = 0$, where y is the meridional coordinate. The wind distributions in the bottom panel of Fig. 7 and the top panel of Fig. 8 are nearly the same. The vector difference between the DLM winds at the center of the vortex is only 0.3 m s^{-1}. The difference is even smaller when the boundary conditions on the eastern and western boundaries are replaced instead (not shown). Therefore the lateral boundaries are sufficiently remote that they do not significantly affect the results of the piecewise inversion.

The importance of the nonlinear terms in the coupled equation system (5) has also been evaluated. The bottom panel of Fig. 8 shows the DLM wind attributable to the same piece of anomalous PV but with the nonlinear terms in (5a) and (5b) (involving the $^1/_2$ factors) omitted. The associated wind field is seen to be only slightly affected by this omission. The vector change in the DLM is only 0.3 m s^{-1}. Thus, the nonlinear terms make only a small contribution to the result, confirming the a priori analysis in section 2 (Fig. 5). The system is effectively linear. So as to avoid arbitrary partitioning, in the remainder of the paper only linear results will be presented.

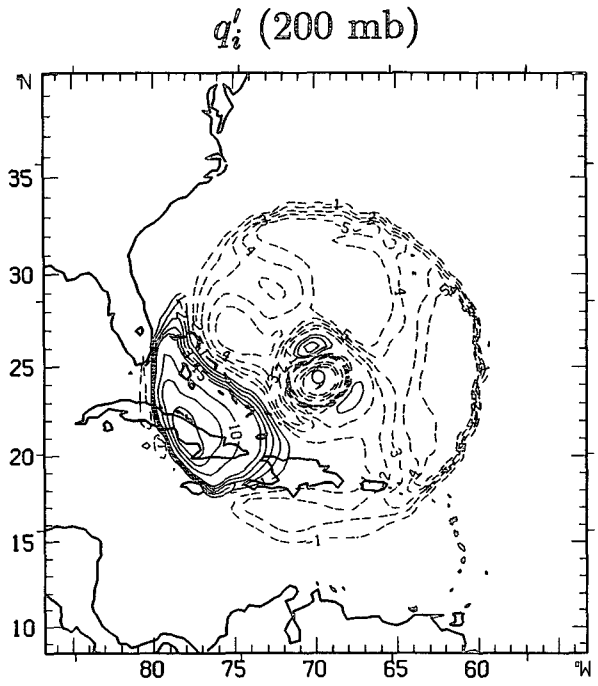

FIG. 6. Same as Fig. 2 but for piece of anomalous potential vorticity q_i' at 200 mb, confined within a disk of radius 1000 km.

Table 1 summarizes results from a set of inversions for pieces of anomalous PV restricted to cylinders of different radii. As in the case just presented, each PV anomaly extends throughout the depth of the atmosphere. The DLM wind at the center of the hurricane attributable to the PV anomalies, as well as the vector difference from the observed storm motion $\mathbf{c}$ are shown. The minimum difference from $\mathbf{c}$ is found for the cylinder of radius 1000 km, with a vector difference of 1.4 m s^{-1}.[4] Cylinders with radii of 1250 and 1500 km, which encompass a greater portion of the PV distribution, are associated with DLM winds that are a poorer approximation to the storm's motion. Since the total analyzed DLM wind at the center of the hurricane

[4] The small discrepancy with the 1.1 m s^{-1} difference quoted above for Fig. 7 is due to the absence of the nonlinear terms in the present solution.

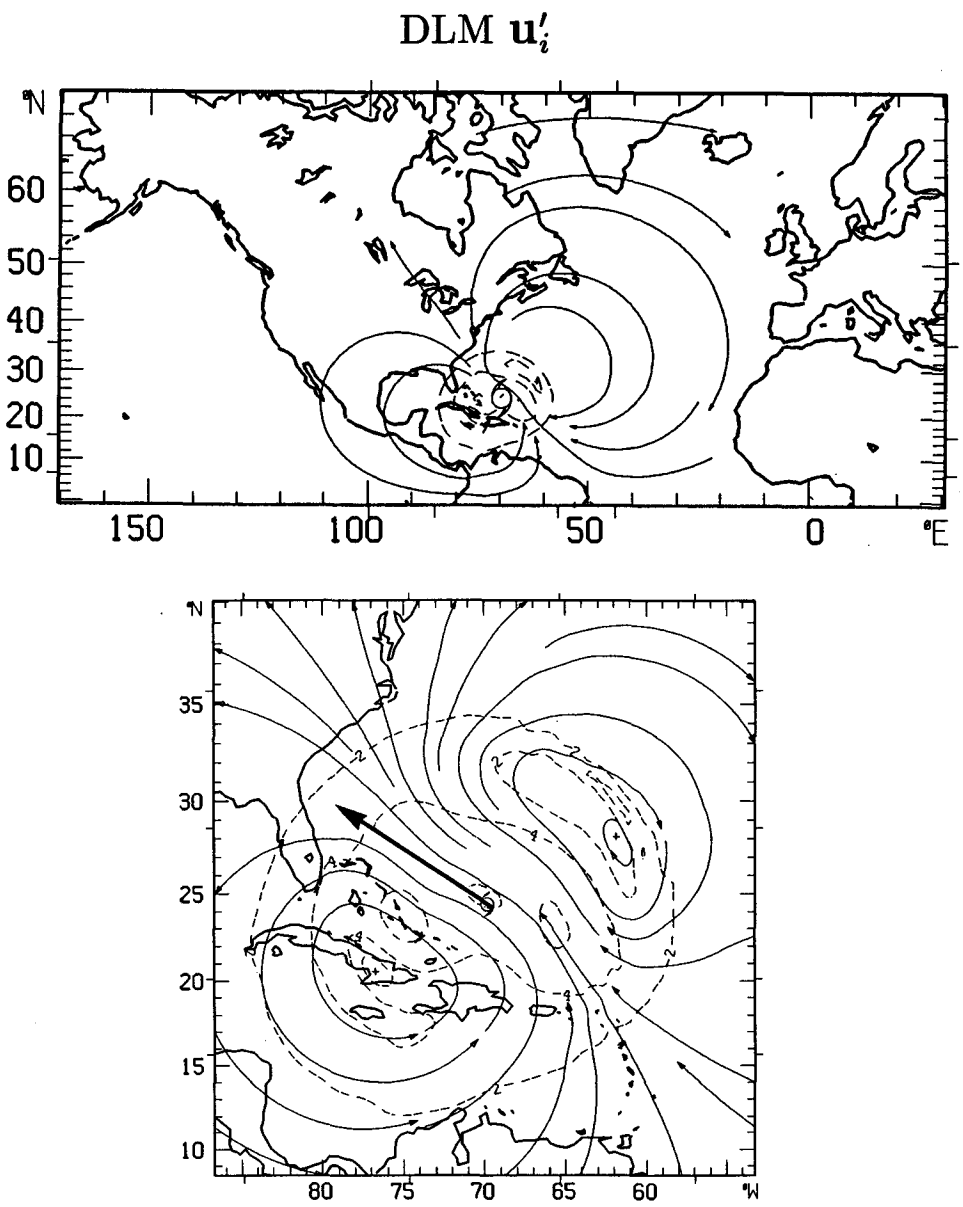

FIG. 7. Same as Fig. 1 but for deep-layer wind anomaly $\mathbf{u}_i'$ attributable to anomalous PV confined within a cylinder of radius 1000 km, extending throughout the depth of the atmosphere. Vector in bottom panel indicates deep-layer mean wind at center of vortex.

differs from **c** by only 0.2 m s^{-1} (see section 1b), PV anomalies confined within a cylinder of sufficiently large radius ($\gg$1500 km) would, however, give a vector difference of that magnitude.

The contribution of PV at each interior mandatory level, as well as the upper and lower boundary θ's, to the total DLM wind at the center of the hurricane attributable to PV anomalies within 1000 km of the vortex center is shown in Fig. 9. Some of the variation in the vertical, particularly the anomalous contribution from PV at 300 mb, may be due to data deficiencies above 400 mb. Only levels 500 mb and above (including the upper boundary) are seen to contribute to the northwestward component of the steering flow; the DLM wind attributable to PV anomalies at these levels is 5.5 m s^{-1} toward 320°, with a vector difference from **c** of 1.0 m s^{-1}.

4. Discussion and conclusions

The upper-level PV anomalies within 1000 km of Gloria's center (see Fig. 6) include both positive values

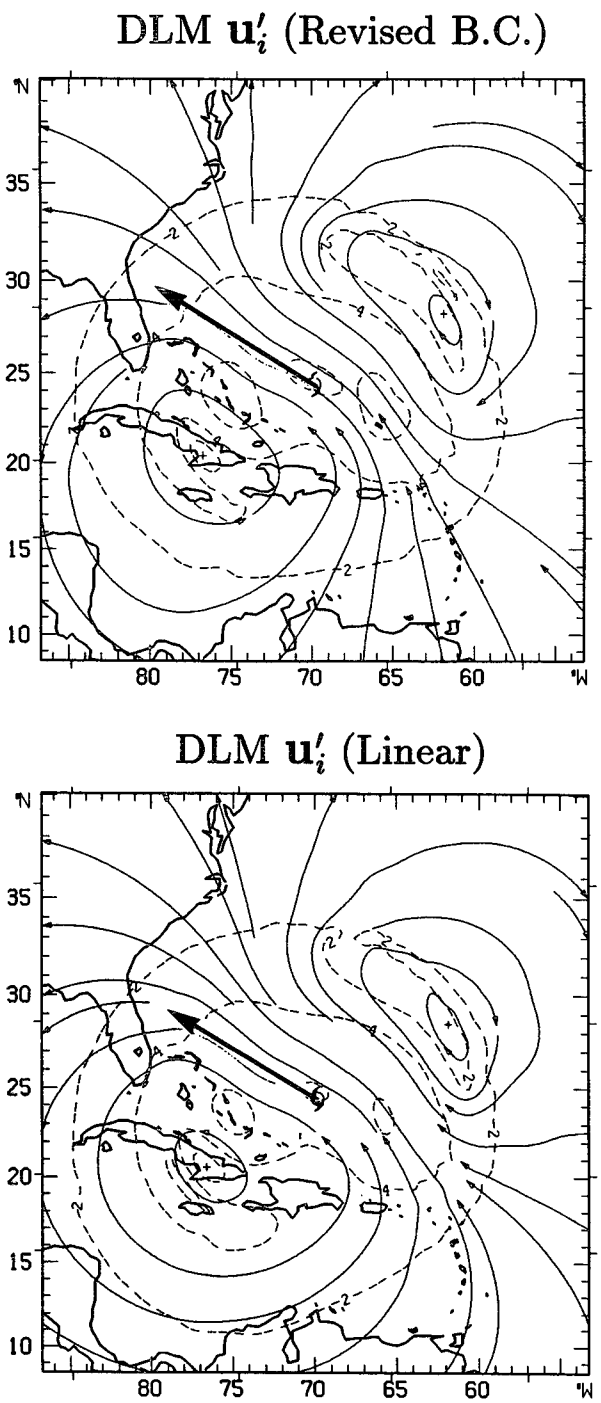

FIG. 8. Same as Fig. 7 but for different boundary conditions (top panel; see text) and for linear piecewise inversion (bottom panel; also see text).

to the southwest, associated with the cold low over Cuba, and negative values to the northeast that may have contributed to the hurricane's northwestward translation. To isolate the effect of the upper-level cold low on Gloria's motion, the piece of anomalous PV restricted to the region shown in the top panel of Fig. 10 is used. The DLM wind asymmetries attributable to a PV anomaly confined within this region and levels 400 mb and above are shown in the bottom panel of Fig. 10. The DLM wind associated with the PV anomaly comprises a single cyclonic gyre with a 3.2 m s^{-1} north-northwestward component across the hurricane's center. The interpretation of this wind as the contribution of the cold low to the DLM flow across Gloria is, however, quite problematic. If another basic-state symmetric vortex were used, then the PV anomaly within the restricted region would change its strength and structure, and the DLM wind attributable to this anomaly would change as well. Although with either basic state, the DLM wind is attributable to a PV anom-

TABLE 1. Deep-layer mean wind at center of Hurricane Gloria (DLM $\mathbf{u}_i'$; toward direction measured clockwise from north) attributable to pieces of anomalous PV confined within cylinders of given radius. Vector difference from the observed storm motion $\mathbf{c}$ (6.2 m s^{-1} toward 313°) is also displayed.

Cylinder radius (km)	DLM $\mathbf{u}_i'$ direction/speed (m s^{-1})	$\lvert\mathbf{u}_i' - \mathbf{c}\rvert$ (m s^{-1})
750	276°/3.8	3.9
1000	301°/6.1	1.4
1250	311°/8.2	2.1
1500	312°/8.9	2.8

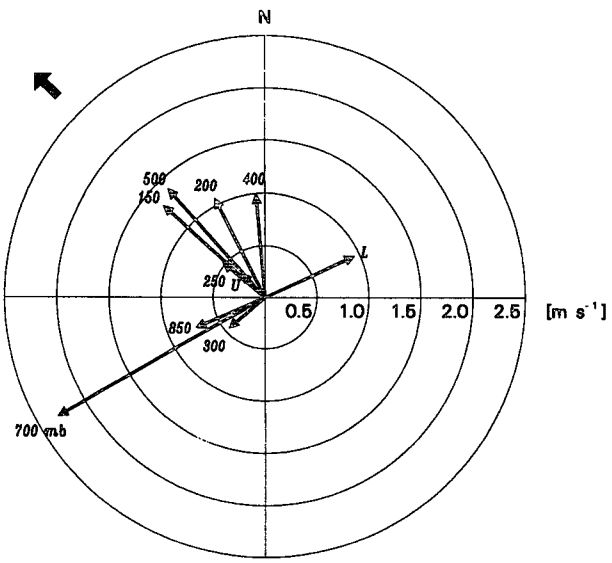

FIG. 9. Contribution of potential vorticity anomaly at each mandatory level from 850 to 150 mb, as well as upper (U; 100 mb) and lower (L; 1000 mb) boundary conditions, to the deep-layer mean wind at Gloria's center attributable to anomalies confined within a cylinder of radius 1000 km. Results from linear piecewise inversion are shown (see text). Large arrow in northwest quadrant indicates, for reference, direction of Gloria's motion.

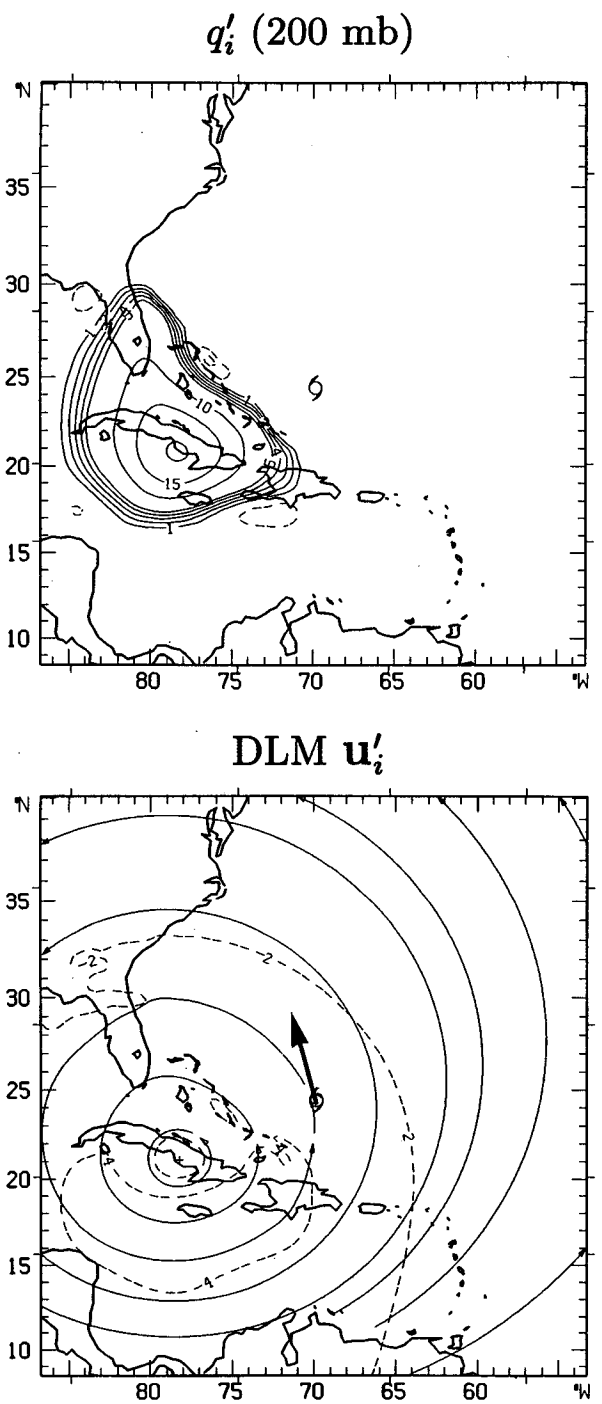

FIG. 10. Piece of anomalous potential vorticity q_i' at 200 mb, restricted to region of cold low over Cuba (top panel; see text), and deep-layer mean wind $\mathbf{u}_i'$ attributable to this anomaly (bottom panel). Vector in bottom panel indicates deep-layer mean wind at center of vortex.

aly in the region of the cold low, the attribution of the flow to the cold low itself is an arbitrary exercise. The same difficulty with interpretation is present in any decomposition, such as that of Davis and Emanuel (1991) and Wu and Emanuel (1995a,b), that removes a climatological (or zonally averaged) basic state. The flow attributed to a given local feature (such as a midlatitude trough) depends on the assumed basic state. This problem was not an issue for the PV anomalies restricted to circularly symmetric regions in section 3, since in those cases the flow across the vortex center (which itself has no symmetric component) is not dependent on the choice of symmetric basic state.

By defining the basic state to be the azimuthally averaged vortex, the present decomposition avoids the ambiguities inherent in removing the climatological flow; the entire wind field at the center of the hurricane can be decomposed. Moreover, the definition of the symmetric vortex as the basic state makes removal of the vortex, as in Wu and Emanuel (1995a,b), unnecessary. With the current methodology the environmental steering flow is modified by the structure of the vortex itself, including its inertial stability. A test of the sensitivity of the results to the presence of the vortex was made, using the same piece of anomalous PV as in Fig. 7, but with the symmetric vortex set artificially to zero in the piecewise inversion. The associated DLM wind at Gloria's center (not shown) differed from that with the vortex included by 1.6 m s^{-1}, indicating that the vortex structure did have an effect on the steering flow. Such a modification to the steering flow could not be included in previous methodologies.

Definition of the basic state as the azimuthally averaged vortex also takes advantage of the weak asymmetries near the hurricane's core and the near-linearity of PV in the environment. As demonstrated in section 3b, the derived system is effectively linear. It was also shown in the same section that for PV anomalies confined within approximately 1000 km of the vortex center the lateral boundaries are sufficiently remote that the results of the piecewise inversion are not significantly affected.

Overall the results confirm the importance of upper-level PV anomalies in hurricane motion as found by Wu and Emanuel (1995a,b). For Gloria the PV anomalies at 500 mb and above within 1000 km of the center are associated with a DLM wind across the vortex that differs from the hurricane's translation velocity by 1.0 m s^{-1}. The wind that steered Gloria can therefore be primarily attributed to PV anomalies within this cylindrical region, with more than five-sixths of Gloria's 6.2 m s^{-1} motion explained; contributions from PV anomalies outside of this region must effectively cancel.

The *current* motion of a hurricane is determined by the winds relatively close to the vortex center. Franklin et al. (1993) found that the best match to Gloria's 12-h motion was with azimuthally averaged DLM winds 65 km from the center. From analyses of 16 Omega dropwindsonde datasets, Franklin et al. (1996) found that the DLM steering envelope lies somewhere within a 333-km radius of a tropical cyclone's center, consistent with the result for Gloria. Therefore, to ob-

tain analyses that accurately represent a hurricane's present motion, wind measurements close to the center and throughout the depth of the atmosphere are required. The hurricane's steering flow will evolve, however, as the PV anomalies in the hurricane's environment that contribute to this flow evolve. The present results therefore imply that in order to improve prediction of short-term *changes* in the environmental flow field that steered Gloria, measurements of upper-level winds and heights are required at least out to 1000 km.[5] The Gulfstream IV jet aircraft, newly acquired by the National Oceanic and Atmospheric Administration and scheduled to begin flying synoptic surveillance missions during the 1996 hurricane season, is the best platform currently available for such measurements.

A larger sample of cases is required to confirm the present results. A total of 15 additional synoptic-flow cases (see section 2 of Franklin et al. 1996), incorporating Omega dropwindsonde observations within about 1000 km of nine tropical storms and hurricanes, are available for analysis. Although these cases do not have as complete data coverage as that for Gloria in the present paper, they do incorporate special enhanced high-density satellite datasets and commercial aircraft reports that supplement operational winds at levels above 400 mb (see section 3 of Franklin et al. 1996). A separate study is planned to use the present methodology on these cases.

Acknowledgments. This research was supported in part by the Office of Naval Research Grant N00014-94-F-0045. This work was supported in part by a grant of HPC time from the Department of Defense HCP Arctic Research Supercomputing Center, CRAY YMP. Discussions with Mr. James Franklin throughout the course of this work have been of considerable value and are greatly appreciated. Additional thanks go to Mr. Franklin, Drs. Mark DeMaria and Steve Lord, and an anonymous reviewer for their valuable comments on an earlier draft of this paper.

APPENDIX

Piecewise Inversion Technique

For a nondivergent flow, Ertel's PV can be written in Mercator coordinates (x, y) as

$$q = \frac{g\kappa\pi}{p}\left[(f + m^2\nabla^2\psi)\frac{\partial^2\phi}{\partial\pi^2} - m^2\frac{\partial^2\psi}{\partial x\partial\pi}\frac{\partial^2\phi}{\partial x\partial\pi} - m^2\frac{\partial^2\psi}{\partial y\partial\pi}\frac{\partial^2\phi}{\partial y\partial\pi}\right], \quad \text{(A1)}$$

where g is the gravitational acceleration, $\kappa = R/c_p$ with R being the gas constant and c_p the specific heat for dry air at constant pressure, $\pi = c_p(p/p_0)^\kappa$ is the Exner function with p the pressure and p_0 the reference pressure of 1000 mb, and m is the map factor for the Mercator projection. The nonlinear balance equation [Eq. (3-81) of Haltiner and Williams (1980)] can be written

$$m^2\nabla^2\phi = m^2\nabla\cdot(f\nabla\psi) + 2m^4\left(\frac{\partial^2\psi}{\partial x^2}\frac{\partial^2\psi}{\partial y^2} - \frac{\partial^2\psi}{\partial x\partial y}\frac{\partial^2\psi}{\partial x\partial y}\right), \quad \text{(A2)}$$

where small corrections due to the earth's curvature have not been presented for simplicity.

Then, the equations for the pieces of PV, ψ', and ϕ' [(5a) and (5b)] become

$$q_i' = \frac{g\kappa\pi}{p}\left[(f + m^2\nabla^2\psi^*)\frac{\partial^2\phi_i'}{\partial\pi^2} + m^2\nabla^2\psi_i'\frac{\partial^2\phi^*}{\partial\pi^2} - m^2\frac{\partial^2\psi_i'}{\partial x\partial\pi}\frac{\partial^2\phi^*}{\partial x\partial\pi} - m^2\frac{\partial^2\psi^*}{\partial x\partial\pi}\frac{\partial^2\phi_i'}{\partial x\partial\pi} - m^2\frac{\partial^2\psi_i'}{\partial y\partial\pi}\frac{\partial^2\phi^*}{\partial y\partial\pi} - m^2\frac{\partial^2\psi^*}{\partial y\partial\pi}\frac{\partial^2\phi_i'}{\partial y\partial\pi}\right], \quad \text{(A3)}$$

where $\psi^* \equiv \bar{\psi} + 1/2\psi'$ and $\phi^* \equiv \hat{\phi} + 1/2\phi'$; and

$$m^2\nabla^2\phi_i' = m^2\nabla\cdot(f\nabla\psi_i') + 2m^4\left(\frac{\partial^2\psi^*}{\partial x^2}\frac{\partial^2\psi_i'}{\partial y^2} + \frac{\partial^2\psi_i'}{\partial x^2}\frac{\partial^2\psi^*}{\partial y^2} - 2\frac{\partial^2\psi^*}{\partial x\partial y}\frac{\partial^2\psi_i'}{\partial x\partial y}\right). \quad \text{(A4)}$$

Following Davis and Emanuel (1991) [their Eq. (A.3)], the linear combination

$$\frac{pq_i'}{g\kappa\pi} + \frac{Sm^2}{2\Omega}\nabla^2\phi_i',$$

where Ω is the earth's angular velocity and the constant S is a characteristic static stability $(\partial^2\phi/\partial\pi^2)$, is manipulated to give

$$\nabla^2\psi_i'^{(n+1)} = \frac{1}{m^2}\left(\frac{Sf}{2\Omega} + \frac{\partial^2\phi^*}{\partial\pi^2}\right)^{-1} \times\left\{\frac{pq_i'}{g\kappa\pi} - N_2(\psi_i'^{(n)}, \phi_i'^{(n)}) - (f + m^2\nabla^2\psi^*) \times\frac{\partial^2\phi_i'^{(n)}}{\partial\pi^2} + \frac{S}{2\Omega}[m^2\nabla^2\phi_i'^{(n)} - N_1(\psi_i'^{(n)})]\right\}, \quad \text{(A5)}$$

where

$$N_1(\psi_i') = m\beta\frac{\partial\psi_i'}{\partial y} + 2m^4\left(\frac{\partial^2\psi^*}{\partial x^2}\frac{\partial^2\psi_i'}{\partial y^2} + \frac{\partial^2\psi_i'}{\partial x^2}\frac{\partial^2\psi^*}{\partial y^2} - 2\frac{\partial^2\psi^*}{\partial x\partial y}\frac{\partial^2\psi_i'}{\partial x\partial y}\right),$$

[5] Presumably, track forecast improvements due to Omega dropwindsonde measurements confined to levels below 400 mb (Burpee et al. 1996) are mostly due to improvements in the initial deep-layer steering.

with β the northward gradient of the Coriolis parameter, and

$$N_2(\psi_i', \phi_i') = -m^2\left(\frac{\partial^2\psi_i'}{\partial x\partial\pi}\frac{\partial^2\phi^*}{\partial x\partial\pi} + \frac{\partial^2\psi^*}{\partial x\partial\pi}\frac{\partial^2\phi_i'}{\partial x\partial\pi} + \frac{\partial^2\psi_i'}{\partial y\partial\pi}\frac{\partial^2\phi^*}{\partial y\partial\pi} + \frac{\partial^2\psi^*}{\partial y\partial\pi}\frac{\partial^2\phi_i'}{\partial y\partial\pi}\right).$$

Similarly, (A3) and (A4) can be manipulated to give

$$\nabla^2\phi_i'^{(n+1)} + \frac{(2\Omega)^2A^2}{S}\frac{\partial^2\phi_i'^{(n+1)}}{\partial\pi^2} = f\nabla^2\psi_i'^{(n+1)} + \frac{N_1(\psi_i'^{(n+1)})}{m^2} + \frac{(2\Omega)^2A^2}{S} \times [(f + m^2\nabla^2\psi^*)^2 + C^2(2\Omega)^2]^{-1}P, \quad \text{(A6)}$$

where

$$P = (f + m^2\nabla^2\psi^*)\left[\frac{pq_i'}{g\kappa\pi} - m^2\nabla^2\psi_i'^{(n+1)}\frac{\partial^2\phi^*}{\partial\pi^2} - N_2(\psi_i'^{(n+1)}, \phi_i'^{(n)})\right] + C^2(2\Omega)^2\frac{\partial^2\phi_i'^{(n)}}{\partial\pi^2},$$

where A^2 and C^2 are positive constants.

At each level the fields are represented as multinested two-dimensional cubic B-splines (Ooyama 1987). The analysis algorithm and methodology are described in section 3 of Franklin et al. (1993). Centered vertical differences are used. From first guesses $\psi_i'^{(0)}$ and $\phi_i'^{(0)}$, the left-hand side of (A5) is solved directly for $\psi_i'^{(1)}$. Then the left-hand side of (A6) is solved iteratively for $\phi_i'^{(1)}$.[6] The system (A5) and (A6) is itself solved iteratively, underrelaxing each updated solution $\psi_i'^{(n+1)}$ and $\phi_i'^{(n+1)}$ by a factor of 0.8 to guarantee convergence. The system is considered to converge if the largest change of streamfunction from one iteration to the next is less than 0.5×10^4 m^2 s^{-1} and of geopotential less than 0.5 m^2 s^{-2}. Convergence also required experimentation with A and C; values of 1.0 and 3.0, respectively, were found to suffice. As found by Davis and Emanuel, the method does not converge unless the condition $q > 0$ is imposed as well. Negative values of q (over small areas of the domain) are set to a small positive value of 1×10^{-8} m^2 s^{-1} K kg^{-1}. When linear results are computed (effectively setting $\psi^* = \bar{\psi}$ and $\phi^* = \hat{\phi}$), the system is first solved nonlinearly to obtain a first guess for the linear solution.

[6] The equation corresponding to (A6) in Davis and Emanuel (1991) is their Eq. (A.4), which involves a variable coefficient multiplying the second-order vertical derivative. The use of a constant coefficient on the left-hand side of (A6) is necessitated by the numerical algorithm currently available for direct inversion, within the multinested finite-element representation, of operators involving the Laplacian.

REFERENCES

Bishop, C. H., and A. J. Thorpe, 1994: Potential vorticity and the electrostatics analogy: Quasi-geostrophic theory. *Quart. J. Roy. Meteor. Soc.*, **120,** 713–731.

Bretherton, F. P., 1966a: Critical layer instability in baroclinic flows. *Quart. J. Roy. Meteor. Soc.*, **92,** 325–334.

——, 1966b: Baroclinic instability and the short wavelength cut-off in terms of potential vorticity. *Quart. J. Roy. Meteor. Soc.*, **92,** 335–345.

Burpee, R. W., J. L. Franklin, S. J. Lord, R. E. Tuleya, and S. D. Aberson, 1996: The impact of Omega dropwindsondes on operational hurricane track forecast models. *Bull. Amer. Meteor. Soc.*, **77,** 925–933.

Davis, C. A., 1992: Piecewise potential vorticity inversion. *J. Atmos. Sci.*, **49,** 1397–1411.

——, and K. A. Emanuel, 1991: Potential vorticity diagnostics of cyclogenesis. *Mon. Wea. Rev.*, **119,** 1925–1953.

Franklin, J. L., S. J. Lord, S. E. Feuer, and F. D. Marks Jr., 1993: The kinematic structure of Hurricane Gloria (1985) determined from nested analyses of dropwindsonde and Doppler radar data. *Mon. Wea. Rev.*, **121,** 2433–2451.

——, S. E. Feuer, J. Kaplan, and S. D. Aberson, 1996: Tropical cyclone motion and surrounding flow relationships: Searching for beta gyres in Omega dropwindsonde datasets. *Mon. Wea. Rev.*, **124,** 64–84.

Haltiner, G. J., and R. T. Williams, 1980: *Numerical Prediction and Dynamic Meteorology.* 2d ed. Wiley, 477 pp.

Hoskins, B. J., 1991: Towards a PV–θ view of the general circulation. *Tellus,* **43A,** 27–35.

——, M. E. McIntyre, and A. W. Robertson, 1985: On the use and significance of isentropic potential vorticity maps. *Quart. J. Roy. Meteor. Soc.*, **111,** 877–946.

Ooyama, K. V., 1987: Scale controlled objective analysis. *Mon. Wea. Rev.*, **115,** 2479–2506.

Shapiro, L. J., 1992: Hurricane vortex motion and evolution in a three-layer model. *J. Atmos. Sci.*, **49,** 140–153.

——, and K. V. Ooyama, 1990: Barotropic vortex evolution on a beta plane. *J. Atmos. Sci.*, **47,** 170–187.

——, and M. T. Montgomery, 1993: A three-dimensional balance theory for rapidly rotating vortices. *J. Atmos. Sci.*, **50,** 3322–3335.

——, and J. L. Franklin, 1995: Potential vorticity in Hurricane Gloria. *Mon. Wea. Rev.*, **123,** 1465–1475.

Thorpe, A. J., and C. H. Bishop, 1995: Potential vorticity and the electrostatics analogy: Ertel–Rossby formulation. *Quart. J. Roy. Meteor. Soc.*, **121,** 1477–1495.

Wu, C.-C., and K. A. Emanuel, 1993: Interaction of a baroclinic vortex with background shear: Application to hurricane movement. *J. Atmos. Sci.*, **50,** 62–76.

——, and ——, 1995a: Potential vorticity diagnosis of hurricane movement. Part I: A case study of Hurricane Bob (1991). *Mon. Wea. Rev.*, **123,** 69–92.

——, and ——, 1995b: Potential vorticity diagnosis of hurricane movement. Part II: Tropical Storm Ana (1991) and Hurricane Andrew (1992). *Mon. Wea. Rev.*, **123,** 93–109.